

Trapped Fermi gases with Rashba spin-orbit coupling in two dimensions

M. Iskin

Department of Physics, Koç University, Rumelifeneri Yolu, 34450 Sarıyer, Istanbul, Turkey.

(Dated: November 15, 2018)

We use the Bogoliubov-de Gennes formalism to analyze harmonically trapped Fermi gases with Rashba-type spin-orbit coupling in two dimensions. We consider both population-balanced and -imbalanced Fermi gases throughout the BCS-BEC evolution, and study the effects of spin-orbit coupling on the spontaneously induced countercirculating mass currents and the associated intrinsic angular momentum. In particular, we find that even a small spin-orbit coupling destabilizes Fulde-Ferrel-Larkin-Ovchinnikov (FFLO)-type spatially modulated superfluid phases as well as the phase-separated states against the polarized superfluid phase. We also show that the continuum of quasiparticle and quasihole excitation spectrum can be connected by zero, one or two discrete branches of interface modes, depending on the number of interfaces between a topologically trivial phase (e.g. locally unpolarized/low-polarized superfluid or spin-polarized normal) and a topologically nontrivial one (e.g. locally high-polarized superfluid) that may be present in a trapped system.

PACS numbers: 05.30.Fk, 03.75.Ss, 03.75.Hh

I. INTRODUCTION

The coupling between a quantum particle's intrinsic angular momentum (spin) and its center of mass (orbital) motion has important consequences in a variety of modern condensed matter problems, ranging from quantum spin Hall systems to topological insulators and topological superconductors [1, 2]. This interaction is referred to as the spin-orbit coupling, and it arises from coupling of the electron's spin to the local magnetic field that is induced in the electron's reference frame, due to the time varying electric field produced by the charged background. Since both the strength and the symmetry of the spin-orbit coupling are mainly determined by the electronic structure of the crystal in condensed matter systems, it is more desirable to engineer spin-orbit coupling in alternative systems that allow more experimental control over its parameters. Given the recent experimental advances in simulating artificial gauge fields with neutral quantum gases [3–6], it is arguable that the prime candidate for engineering spin-orbit couplings in a controllable many-body setting seems to be the atomic ones. For instance, this has recently been achieved first with bosonic [3, 4] and then fermionic [5, 6] atomic gases, by coupling the momentum of atoms to their spin, via Raman dressing of atomic hyperfine states with a pair of laser beams. While the symmetry of all of the experimentally engineered spin-orbit couplings is so far an equal mixture of Rashba and Dresselhaus types, theoretical proposals for creating unequal combinations are also underway.

Since the realization of spin-orbit coupled BECs [3], there has been growing theoretical interest in studying spin-orbit coupled Fermi gases, even prior to their very recent realization [5, 6]. For population-balanced uniform systems, it has been shown that the BCS-BEC evolution is a crossover, and this evolution can be driven either by increasing the interparticle interaction strength for a fixed spin-orbit coupling or by increasing the spin-orbit coupling for a fixed interaction strength (no matter how small the interaction strength is) [7–12]. On the other hand, for population-imbalanced uniform systems, the BCS-BEC evolution is not a crossover, and quantum phase transitions are found between thermodynamically

stable and topologically distinct gapped and gapless superfluid phases. These phases are distinguished in momentum space by their numbers of zero-energy points, rings or surfaces (depending on the type of spin-orbit coupling) in their quasiparticle/quasihole excitation spectrum [13–19].

In direct application to atomic systems, the thermodynamic phase diagrams obtained in these works can be easily used to extract information about the trapped Fermi gases, at least within the semiclassical local-density approximation [20–23]. This commonly used approximation works better and better when the number of fermions is increased towards infinity, as the finite-size effects become negligible. However, a fully quantum mechanical method, e.g. Bogoliubov-de Gennes (BdG) formalism, suits better for studying finite-size effects. Therefore, in this paper we develop a self-consistent BdG formalism to study harmonically trapped Fermi gases with spin-orbit coupling. We only consider the Rashba-type spin-orbit coupling in two dimensions due to its numerical simplicity (see Sec. II A), and hope that some of our qualitative conclusions hold in three dimensions as well. However, we note that, given the recent realization of two-dimensional Fermi gases [24, 25], it may also be possible to engineer spin-orbit coupling in reduced dimensions. Our main focus here is about the spin-orbit coupling induced countercirculating mass currents, where we systematically analyze their dependence on the spin-orbit coupling, two-body binding energy and population imbalance. We note that induced currents in trapped atomic systems have recently been discussed for an optical lattice model [26]. While the Hamiltonian used and the BdG formalism developed in this work is completely different, our results are in qualitative agreement with each other when there is an overlap.

The rest of the manuscript is organized as follows. In Sec. II, we generalize the BdG formalism to spin-orbit coupled Fermi gases, and derive the self-consistency (order parameter and number) equations, probability current density, and the associated angular momentum. These equations are numerically solved and analyzed in Sec. III, and our main findings are briefly summarized in Sec. IV.

II. BOGOLIUBOV-DE GENNES FORMALISM

Our analysis is based on the self-consistent BdG formalism, which enables us to include the single-particle quantum harmonic oscillator solutions exactly in the real space mean-field Hamiltonian density. For this purpose, let us first describe the generalization of this theoretical framework to two-dimensional trapped Fermi gases with Rashba-type spin-orbit coupling.

A. Hamiltonian and self-consistency equations

To describe the spin-orbit coupled Fermi gases with attractive and short-range interactions, we use the Hamiltonian density (in units of $\hbar = k_B = 1$), $H(\mathbf{r}) = \sum_{\sigma,\sigma'} \psi_{\sigma'}^{\dagger}(\mathbf{r}) K_{\sigma\sigma'}(\mathbf{r}) \psi_{\sigma'}(\mathbf{r}) + \Delta(\mathbf{r}) \psi_{\uparrow}^{\dagger}(\mathbf{r}) \psi_{\downarrow}^{\dagger}(\mathbf{r}) + \Delta^*(\mathbf{r}) \psi_{\downarrow}(\mathbf{r}) \psi_{\uparrow}(\mathbf{r})$, where the operators $\psi_{\sigma}^{\dagger}(\mathbf{r})$ and $\psi_{\sigma}(\mathbf{r})$ create and annihilate a pseudo-spin σ fermion at position \mathbf{r} , respectively, and $\Delta(\mathbf{r})$ is the mean-field superfluid order parameter. The diagonal operator $K_{\sigma\sigma}(\mathbf{r}) = -\nabla^2/(2M) - \mu_{\sigma} + V(r)$ includes both the kinetic energy and the harmonic trapping potential $V(r) = M\omega^2 r^2/2$, where M is the mass and μ_{σ} is the chemical potential of σ fermions, and ω is the trapping frequency. The off-diagonal operator $K_{\uparrow\downarrow}(\mathbf{r}) = K_{\downarrow\uparrow}^{\dagger}(\mathbf{r}) = \alpha(p_y + ip_x)$ is the Rashba-type spin-orbit coupling, where $\alpha \geq 0$ is its strength and $p_j = -i\partial/\partial j$ is the momentum operator. In the polar coordinate system (r, θ) , this term becomes $K_{\uparrow\downarrow}(\mathbf{r}) = e^{-i\theta}[\partial/\partial r - i\partial/(\partial\theta)]$, which makes the Rashba-type spin-orbit coupling numerically much easier to simulate in two dimensions due to its rotational invariance.

The mean-field Hamiltonian can be diagonalized via a generalized Bogoliubov-Valatin transformation, and the resultant BdG equation can be written as $H(\mathbf{r})\varphi_n(\mathbf{r}) = \varepsilon_n\varphi_n(\mathbf{r})$, where

$$H(\mathbf{r}) = \begin{bmatrix} K_{\uparrow\uparrow}(\mathbf{r}) & K_{\uparrow\downarrow}(\mathbf{r}) & 0 & \Delta(\mathbf{r}) \\ K_{\downarrow\uparrow}(\mathbf{r}) & K_{\downarrow\downarrow}(\mathbf{r}) & -\Delta(\mathbf{r}) & 0 \\ 0 & -\Delta^*(\mathbf{r}) & -K_{\uparrow\uparrow}^*(\mathbf{r}) & -K_{\uparrow\downarrow}^*(\mathbf{r}) \\ \Delta^*(\mathbf{r}) & 0 & -K_{\downarrow\uparrow}^*(\mathbf{r}) & -K_{\downarrow\downarrow}^*(\mathbf{r}) \end{bmatrix} \quad (1)$$

is the Hamiltonian matrix given in the $\varphi_n(\mathbf{r}) = [u_{\uparrow n}(\mathbf{r}), u_{\downarrow n}(\mathbf{r}), v_{\uparrow n}(\mathbf{r}), v_{\downarrow n}(\mathbf{r})]^T$ basis, and $\varepsilon_n \geq 0$ are the energy eigenvalues. The mean-field superfluid order parameter $\Delta(\mathbf{r}) = g\langle\psi_{\uparrow}(\mathbf{r})\psi_{\downarrow}(\mathbf{r})\rangle$, where $g \geq 0$ is the strength of the attractive interaction between \uparrow and \downarrow fermions, and $\langle\cdots\rangle$ is the thermal average, becomes $\Delta(\mathbf{r}) = g\sum_n [u_{\uparrow n}(\mathbf{r})v_{\downarrow n}^*(\mathbf{r})f(-\varepsilon_n) + u_{\downarrow n}(\mathbf{r})v_{\uparrow n}^*(\mathbf{r})f(\varepsilon_n)]$. Here, $f(x) = 1/(e^{x/T} + 1)$ is the Fermi function and T is the temperature. We may relate g to the energy $\varepsilon_b \leq 0$ of the two-body bound state between an \uparrow and a \downarrow fermion in vacuum via the relation, $1/g = \sum_{\mathbf{k}} 1/(2\varepsilon_{\mathbf{k}} - \varepsilon_b)$, where $\varepsilon_{\mathbf{k}} = k^2/(2M)$ is the kinetic energy. This leads to $g = 4\pi/[M \ln(1 + 2\varepsilon_c/|\varepsilon_b|)]$, where ε_c is the energy cutoff used in the \mathbf{k} -space integration (ε_c is specified below in Sec. III). The order parameter equation has to be solved self-consistently with the number equations $N_{\sigma} = \int d\mathbf{r} n_{\sigma}(\mathbf{r})$,

where $n_{\sigma}(\mathbf{r}) = \langle\psi_{\sigma}^{\dagger}(\mathbf{r})\psi_{\sigma}(\mathbf{r})\rangle$ is the local density of σ fermions. Using the Bogoliubov-Valatin transformations, we obtain $n_{\sigma}(\mathbf{r}) = \sum_n [|u_{\sigma n}(\mathbf{r})|^2 f(\varepsilon_n) + |v_{\sigma n}(\mathbf{r})|^2 f(-\varepsilon_n)]$. Thus, the order parameter and number equations form a closed set, determining $\Delta(\mathbf{r})$ and μ_{σ} for any given ε_b , α and T .

We take advantage of the rotational invariance of the Hamiltonian, and conveniently expand the normalized wave functions as $u_{\uparrow n}(\mathbf{r}) = \sum_n c_{\uparrow mn} \phi_{nm}(\mathbf{r})$ and $v_{\uparrow n}(\mathbf{r}) = \sum_n d_{\uparrow mn} \phi_{n,m+1}(\mathbf{r})$ for the \uparrow components, and $u_{\downarrow n}(\mathbf{r}) = \sum_n c_{\downarrow mn} \phi_{n,m+1}(\mathbf{r})$ and $v_{\downarrow n}(\mathbf{r}) = \sum_n d_{\downarrow mn} \phi_{nm}(\mathbf{r})$ for the \downarrow ones. Here, $\phi_{nm}(\mathbf{r}) = R_{nm}(r)\Theta_m(\theta)$ are the solutions for the single-particle quantum harmonic oscillator problem, where $R_{nm}(r) = \beta^{|m|+1} \sqrt{2n!/(n+|m|)!} e^{-\beta^2 r^2/2} r^{|m|} L_n^{|m|}(\beta^2 r^2)$ is the radial, and $\Theta_m(\theta) = e^{im\theta}/\sqrt{2\pi}$ is the angular part of the wave function. The quantum numbers $n = 0, 1, 2, \dots, \infty$ and $m = 0, \pm 1, \pm 2, \dots, \pm\infty$ correspond, respectively, to the radial and angular degrees of freedom, $\beta = \sqrt{M\omega}$, and $L_n^{|m|}(x)$ is the associated Laguerre polynomial. This particular choice allow us to decouple the BdG equations into independent subspaces of m sectors as shown below.

Using the orthonormality relations $\int_0^{\infty} r dr R_{nm}(r) R_{n'm}(r) = \delta_{nn'}$ and $\int_0^{2\pi} d\theta \Theta_m^*(\theta) \Theta_m(\theta) = 1$, where $\delta_{nn'}$ is the Kronecker delta, this procedure reduces the BdG equation given in Eq. (1) to a $4(n_{max} + 1) \times 4(n_{max} + 1)$ matrix eigenvalue problem,

$$\sum_{n'} \begin{pmatrix} K_{\uparrow m}^{nn'} & -S_{-m-1}^{nn'} & 0 & \Delta_m^{nn'} \\ -S_{-m-1}^{nn'} & K_{\downarrow, m+1}^{nn'} & -\Delta_{m+1}^{nn'} & 0 \\ 0 & -\Delta_{m+1}^{nn'} & -K_{\uparrow, m+1}^{nn'} & S_m^{nn'} \\ \Delta_m^{nn'} & 0 & S_m^{nn'} & -K_{\downarrow m}^{nn'} \end{pmatrix} \begin{pmatrix} c_{\uparrow mn'} \\ c_{\downarrow mn'} \\ d_{\uparrow mn'} \\ d_{\downarrow mn'} \end{pmatrix} = \varepsilon_{mn} \begin{pmatrix} c_{\uparrow mn} \\ c_{\downarrow mn} \\ d_{\uparrow mn} \\ d_{\downarrow mn} \end{pmatrix}, \quad (2)$$

for each m sector, if we allow $0 \leq n \leq n_{max}$ states (n_{max} is specified below in Sec. III). Here, $K_{\sigma m}^{nn'} = [\omega(2n + |m| + 1) - \mu_{\sigma}] \delta_{nn'}$ are the single-particle terms, $S_m^{nn'} = -\alpha \int_0^{\infty} r dr R_{n,m+1}(r) (\partial/\partial r - m/r) R_{n'm}(r)$ are the spin-orbit coupling terms leading to $S_m^{nn'} = -\alpha \int_0^{\infty} r dr R_{n,m+1}(r) [\beta^2 r + (|m| - m)/r] R_{n'm}(r) + 2\alpha\beta\sqrt{n' + |m| + 1} \int_0^{\infty} r dr R_{n,m+1}(r) R_{n',|m|+1}(r)$, and $\Delta_m^{nn'} = \int_0^{\infty} r dr \Delta(r) R_{nm}(r) R_{n'm}(r)$ are the pairing terms.

The same procedure also reduces the order-parameter equation to

$$\Delta(r) = \frac{g}{2\pi} \sum_{mnn'} [c_{\downarrow mn} d_{\uparrow mn'} R_{n,m+1}(r) R_{n',m+1}(r) f(\varepsilon_{mn}) + c_{\uparrow mn} d_{\downarrow mn'} R_{nm}(r) R_{n'm}(r) f(-\varepsilon_{mn})], \quad (3)$$

where $\Delta(r) = \int_0^{2\pi} d\theta \widehat{\Delta}(\mathbf{r})/(2\pi)$ is averaged over the angular direction (recall the rotational invariance of the system) and it is assumed to be real without losing generality, and the angular averaged local-density equations $n_{\sigma}(r) =$

$\int_0^{2\pi} d\hat{\mathbf{r}} n_\sigma(\mathbf{r})/(2\pi)$ to

$$n_\uparrow(r) = \frac{1}{2\pi} \sum_{mnn'} [c_{\uparrow mn} c_{\uparrow mn'} R_{nm}(r) R_{n'm}(r) f(\varepsilon_{mn}) + d_{\uparrow mn} d_{\uparrow mn'} R_{n,m+1}(r) R_{n',m+1}(r) f(-\varepsilon_{mn})], \quad (4)$$

$$n_\downarrow(r) = \frac{1}{2\pi} \sum_{mnn'} [c_{\downarrow mn} c_{\downarrow mn'} R_{n,m+1}(r) R_{n',m+1}(r) f(\varepsilon_{mn}) + d_{\downarrow mn} d_{\downarrow mn'} R_{nm}(r) R_{n'm}(r) f(-\varepsilon_{mn})]. \quad (5)$$

We recall that the sums are only over the quasiparticle states with $\varepsilon_{mn} \geq 0$. Using the orthonormality relations, we also obtain the total number of σ fermions as $N_\sigma = \sum_{mn} [c_{\sigma mn}^2 f(\varepsilon_{mn}) + d_{\sigma mn}^2 f(-\varepsilon_{mn})]$. We emphasize that these mean-field equations can be used to investigate the low temperature properties of the system for all values of ε_b and α , but they provide only a qualitative description of the system outside of the weak-coupling regime, i.e. in the BCS-BEC evolution.

B. Countercirculating mass currents

Once the quasiparticle energies and the corresponding wave functions are obtained, through self-consistently solving the BdG equations discussed above, it is a straightforward task to calculate other observables of interest. For instance, next we illustrate how we obtain the density of spin-orbit coupling induced currents, as well as the intrinsic angular momentum associated with the flow of particles.

Similar to the usual $\alpha = 0$ treatment, the quantum mechanical probability-current operator for σ fermions can be identified from the continuity equation. While the presence of a spin-orbit coupling leads to additional terms in the total particle current operator, these terms do not contribute to the current since the expectation value $\langle \psi_\uparrow^\dagger(\mathbf{r}) \psi_\downarrow(\mathbf{r}) \rangle = 0$. Therefore, using the Bogoliubov-Valatin transformation, the local current density $\mathbf{J}_\sigma(\mathbf{r}) = [1/(2Mi)] \langle \psi_\sigma^\dagger(\mathbf{r}) \nabla \psi_\sigma(\mathbf{r}) - H.c. \rangle$ circulating around the center of the trapping potential becomes $\mathbf{J}_\sigma(\mathbf{r}) = [1/(2Mi)] \sum_n [u_{\sigma n}^*(\mathbf{r}) \nabla u_{\sigma n}(\mathbf{r}) f(\varepsilon_n) + v_{\sigma n}^*(\mathbf{r}) \nabla v_{\sigma n}(\mathbf{r}) f(-\varepsilon_n) - H.c.]$, where $H.c.$ is the Hermitian conjugate. Since $\mathbf{J}_\sigma(\mathbf{r})$ circulates along the $\hat{\theta}$ direction, i.e. $\mathbf{J}_\sigma(\mathbf{r}) = J_\sigma(r) \hat{\theta}$, we find

$$J_\uparrow(r) = \frac{1}{2\pi M r} \sum_m \left\{ m \left[\sum_n c_{\uparrow mn} R_{nm}(r) \right]^2 f(\varepsilon_{mn}) - (m+1) \left[\sum_n d_{\uparrow mn} R_{n,m+1}(r) \right]^2 f(-\varepsilon_{mn}) \right\}, \quad (6)$$

$$J_\downarrow(r) = \frac{1}{2\pi M r} \sum_m \left\{ (m+1) \left[\sum_n c_{\downarrow mn} R_{n,m+1}(r) \right]^2 f(\varepsilon_{mn}) - m \left[\sum_n d_{\downarrow mn} R_{nm}(r) \right]^2 f(-\varepsilon_{mn}) \right\}, \quad (7)$$

for the strengths of the current densities.

In this paper, we are also interested in the intrinsic angular momentum associated with the spontaneous flow of

spin-orbit coupling induced particle flow. The angular momentum is along the $\hat{\mathbf{z}}$ direction, and its density $\ell_\sigma(r)$ can be shown to be related to the strength of the current density via $\ell_\sigma(r) = M r J_\sigma(r)$. Using the orthonormality relations, we obtain the total angular momentum of σ fermions $L_\sigma = \int d\mathbf{r} \ell_\sigma(r)$ as

$$L_\uparrow = \sum_{mn} [m c_{\uparrow mn}^2 f(\varepsilon_{mn}) - (m+1) d_{\uparrow mn}^2 f(-\varepsilon_{mn})], \quad (8)$$

$$L_\downarrow = \sum_{mn} [(m+1) c_{\downarrow mn}^2 f(\varepsilon_{mn}) - m d_{\downarrow mn}^2 f(-\varepsilon_{mn})]. \quad (9)$$

Having generalized the theoretical BdG framework for the trapped two-dimensional Fermi gases with Rashba-type spin-orbit coupling, next we discuss our numerical results that comes out of this formalism.

III. NUMERICAL RESULTS

In our numerical calculations, we set a large energy cutoff $\varepsilon_c \gg \varepsilon_F$, and numerically solve the self-consistency Eqs. (2)-(5). Here, $\varepsilon_F = k_F^2/(2M) = M\omega^2 r_F^2/2$ is a characteristic Fermi-energy scale, where r_F is the Thomas-Fermi radius and k_F is the Fermi momentum corresponding to the total density of fermions at the center of the trap when $g = 0$, i.e. $n_\uparrow(0) + n_\downarrow(0) = k_F^2/(2\pi)$ at $r = 0$. We also relate the energy cutoff and Fermi energy to the occupation of harmonic oscillator levels as $\varepsilon_c = \omega(N_c + 1)$ and $\varepsilon_F = \omega(N_F + 1)$, respectively, where $N_c \gg N_F$. This leads to a total of $N = (N_F + 1)(N_F + 2)$ fermions, and therefore, $\varepsilon_F \approx \omega\sqrt{N}$ when $N_F \gg 1$. In addition, in order to be consistent with the energy cutoff, we choose $n_{max} = (N_c - |m|)/2$ as the maximum radial quantum number for a given m , and $m_{max} = N_c$ as the maximum angular quantum number. In particular, here we choose $N_F = 25$ and $\varepsilon_c = 7\varepsilon_F$, which corresponds to a total of $N = 702$ fermions and $N_c = 181$. We checked that these values are sufficiently high for the parameter regime of our interest, since our results for the order parameter and density of fermions agree well (within a few percent) with those obtained within the local-density approximation.

Next, we present our numerical results for population-balanced ($P = 0$) as well as -imbalanced ($P \neq 0$) Fermi gases, where $P = (N_\uparrow - N_\downarrow)/N$ is the population-imbalance parameter.

A. Population-balanced Fermi gases

In Fig. 1, we set $P = 0$ and $|\varepsilon_b| = 0.2\varepsilon_F$, and show $\Delta(r)$, $n_\sigma(r)$ and $J_\sigma(r)$ as a function of r , for a number of α values. First of all, since spin-orbit coupling increases the low-energy density of states, which is similar to what happens in the thermodynamic systems [9, 10], increasing α monotonically increases $n_\sigma(r)$ near the center of the trap, and as a result of which the Fermi gas shrinks. For instance, when α is increased from 0 to k_F/M , the central $n_\sigma(r)$ increases by %25, going from $k_F^2/(4\pi)$ to approximately $5k_F^2/(16\pi)$. However,

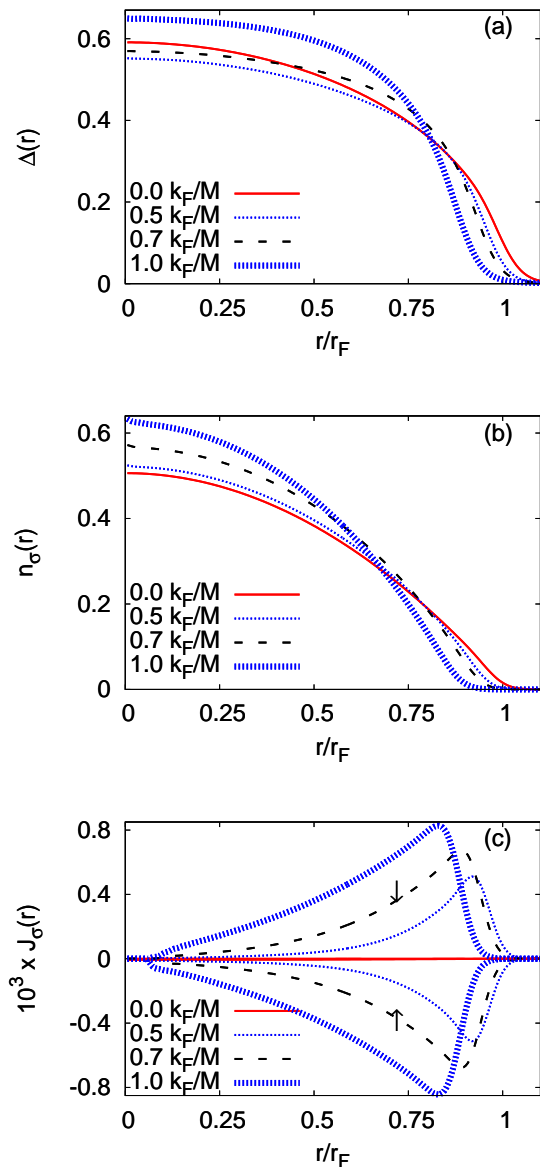


FIG. 1: (color online) Population-balanced ($P = 0$) Fermi gas. We set the two-body binding energy to $|\varepsilon_b| = 0.2\varepsilon_F$ and show (a) the order parameter $\Delta(r)$ (in units of ε_F), (b) density $n_\sigma(r)$ [in units of $k_F^2/(2\pi)$], and (c) probability current distribution $J_\sigma(r)$ (in units of k_F^3/M) profiles as a function of radial distance r (in units of r_F), for a number of spin-orbit coupling strengths α .

the corresponding $\Delta(r)$ has a nonmonotonic dependence on α . We find that the central $\Delta(r)$ decreases slightly until a critical value of $\alpha \approx 0.5k_F/M$ is reached, beyond which $\Delta(r)$ increases with increasing α . The increase in $\Delta(r)$ is again mainly a consequence of increased density of states.

As we discuss below, the presence of a Rashba-type spin-orbit coupling spontaneously induces countercirculating mass currents. This is clearly seen in Fig. 1(c), where the \uparrow and \downarrow fermions are rotating around the center of the trap in opposite directions but with equal speed, due to the time-reversal

symmetry of the parent Hamiltonian. We note that the directions of circulating currents are determined by the chirality of the spin-orbit coupling, and the \uparrow and \downarrow currents would reverse directions if $K_{\uparrow\downarrow}(\mathbf{r}) = \alpha(p_y - ip_x)$ is used. We see that $J_\downarrow(r) = -J_\uparrow(r)$ has a nonmonotonic dependence on r : it gradually increases from 0 as a function of r making a peak at an intermediate distance near the edge of the system, beyond which it rapidly decreases to 0. The peak value of $J_\sigma(r)$ increases with increasing α , since a nonzero α is what causes counter currents to circulate to begin with. In addition, since increasing α shrinks the Fermi gas, the radial location of the peak moves inwards towards the trap center.

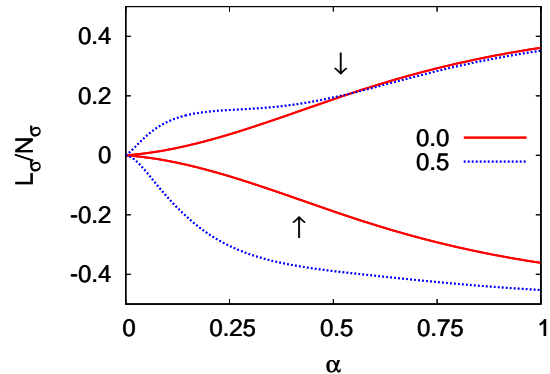


FIG. 2: (color online) We set the two-body binding energy to $|\varepsilon_b| = 0.2\varepsilon_F$, and show the total angular momentum per σ fermion L_σ/N_σ (in units of $\hbar = 1$) as a function of spin-orbit coupling strengths α (in units of k_F/M), for both population-balanced ($P = 0$) and -imbalanced ($P = 0.5$) Fermi gases.

In Fig. 2, we show the total angular momentum (per particle) associated with the particle flow as a function of α . When $P = 0$, we find that $L_\downarrow/N_\downarrow = -L_\uparrow/N_\uparrow$ monotonically increases from 0, and we expect it to saturate at 0.5 when $\alpha \gg k_F/M$. (Since our energy cutoff is not sufficiently high compared to the energy associated with the spin-orbit coupling when $\alpha \gtrsim 1.2$, we could not verify this expectation.) We note that the angular momentum of rotating atomic systems have so far only been achieved indirectly, by observing the shift of the radial quadrupole modes. While this technique was initially used for rotating atomic BECs [27, 28], it has recently been applied to the rotating fermionic superfluids in the BCS-BEC crossover [29]. We believe a similar technique could be used for measuring the intrinsic angular momentum of spin-orbit coupled Fermi gases, which may provide an indirect evidence for countercirculating mass currents.

The origin of spontaneously induced countercirculating mass currents can be understood via a direct correspondence with the $p_x + ip_y$ -superfluids/superconductors [26]. In these p -wave systems, the mass current is associated with the chirality of Cooper pairs [30], and this is easily seen by noting that the chiral p -wave order parameter $\Delta_{\mathbf{k}} \propto (\hat{x} \pm i\hat{y}) \cdot \mathbf{k}$, where \mathbf{k} is the relative momentum of a Cooper pair, is an eigenfunction of the orbital angular momentum with eigenvalue $\pm\hbar$. This explains our findings since it can be shown that the order param-

eter of Fermi gases with Rashba-type spin-orbit coupling and s -wave contact interactions has chiral p -wave symmetry [9]. However, unlike the chiral p -wave systems which break time-reversal symmetry and belong to the topological class of integer quantum Hall systems, spin-orbit coupled Fermi gases preserve time-reversal symmetry just like quantum spin Hall systems, and therefore, they exhibit spontaneously induced countercirculating \uparrow and \downarrow mass currents.

B. Population-imbalanced Fermi gases

Having presented our numerical results for the population-balanced Fermi gases, next we discuss the effects of population imbalance on the system. In Fig. 3, we set $P = 0.5$ and $|\varepsilon_b| = 0.2\varepsilon_F$, and show $\Delta(r)$, $n_\sigma(r)$ and $J_\sigma(r)$ as a function of r , for a number of α values. When $\alpha = 0$, we see that $n_\uparrow(r) = n_\downarrow(r)$ for $r \lesssim 0.25r_F$, $n_\uparrow(r) > n_\downarrow(r) \neq 0$ for $0.25r_F \lesssim r \lesssim 0.8r_F$, and $n_\uparrow(r) > n_\downarrow(r) = 0$ for $r \gtrsim 0.8r_F$. Therefore, the central region corresponds to an unpolarized superfluid, and the excess spin-polarized \uparrow fermions are expelled towards the edge of the system, i.e. paired \uparrow and \downarrow fermions and unpaired normal \uparrow fermions are phase separated, with a coexistence region (i.e. a polarized superfluid) in between.

For small $\alpha \neq 0$, we see that the polarized superfluid region rapidly expands towards the central region, and the system mostly consists of a polarized superfluid near the center of the trap which is phase separated from a spin-polarized normal \uparrow fermions residing near the edge. For larger α values, the spin-polarized \uparrow gas gives its way to the polarized superfluid, and the entire system eventually becomes a polarized superfluid beyond a critical α . This happens around $\alpha \gtrsim 0.5k_F/M$ when $P = 0.5$ and $|\varepsilon_b| = 0.2\varepsilon_F$. We note in passing that these findings are consistent with the recent works on thermodynamic phase diagrams [14–19], where the phase separated state was shown to become gradually unstable against the polarized superfluid phase as α increases from 0.

In addition, these recent works on thermodynamic systems showed that, unlike the $\alpha = 0$ limit where the unpolarized superfluid phase is gapped and polarized superfluid phase is gapless, $\alpha \neq 0$ allows the possibility of having a gapped polarized superfluid phase up to a critical polarization, depending on the particular value of α [14–19]. Therefore, when $\alpha \neq 0$, in contrast to the topologically trivial unpolarized and low-polarized superfluid phases, the polarized superfluid phase with sufficiently high polarization becomes topologically nontrivial, and has gapless quasiparticle/quasihole excitations. Note in a trapped system that the topologically nontrivial locally high-polarized superfluid phase is sandwiched between topologically trivial phases (locally unpolarized/low-polarized superfluid and spin-polarized normal) for small α .

The corresponding $\Delta(r)$ are shown in Fig. 3 (b). When $\alpha = 0$, we see that $\Delta(r)$ oscillates with multiple sign changes, which is reminiscent of FFLO-type spatially-modulated superfluid phases. Similar to the $P = 0$ case, for small $\alpha \neq 0$, the central $\Delta(r)$ decreases slightly until a critical value of $\alpha \approx 0.7k_F/M$ is reached, beyond which $\Delta(r)$ increases with

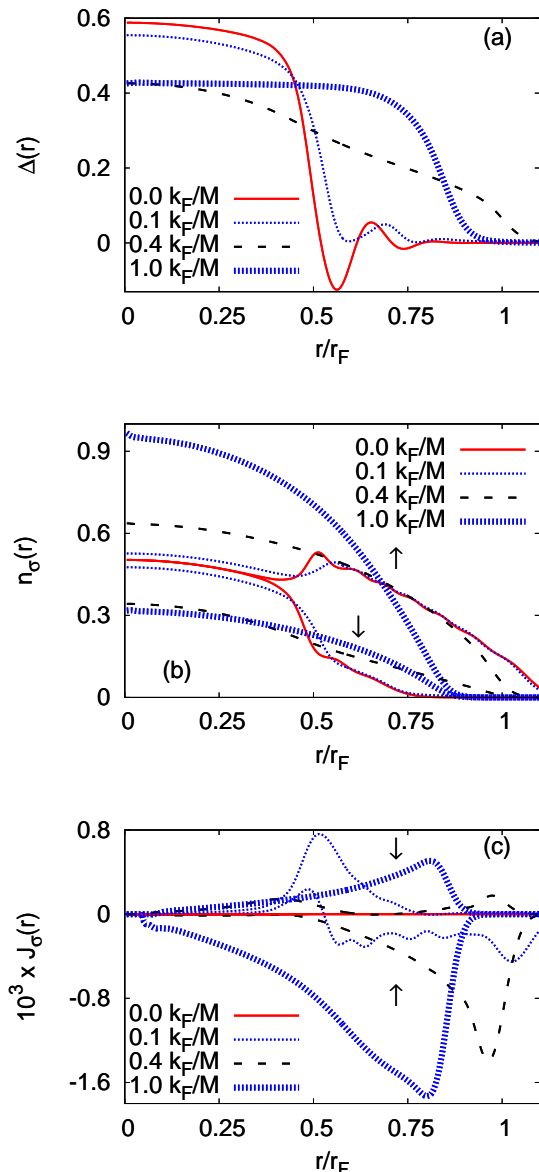


FIG. 3: (color online) Population-imbalanced ($P = 0.5$) Fermi gas. We set the two-body binding energy to $|\varepsilon_b| = 0.2\varepsilon_F$, and show (a) the order parameter $\Delta(r)$ (in units of ε_F), (b) density $n_\sigma(r)$ [in units of $k_F^2/(2\pi)$], and (c) probability current distribution $J_\sigma(r)$ (in units of k_F^3/M) profiles as a function of radial distance r (in units of r_F), for a number of spin-orbit coupling strengths α .

increasing α . More importantly, the spatial modulations of $\Delta(r)$ rapidly disappear with increasing α , and $\Delta(r)$ first becomes finite and then gradually increases near the edge of the system. This again indicates that the polarized superfluid phase expands towards the edge of the system as α gets larger. For larger α values, $\Delta(r)$ gradually increases everywhere, and it eventually becomes nearly flat for a substantial region of the system, except for a small region around the edge. These findings suggest that FFLO-type modulated phases, which are known to play a minor role in the thermodynamic phase dia-

grams when $\alpha = 0$, becomes irrelevant for sufficiently large α . Therefore, our work provides supporting evidence that the recent thermodynamic phase diagrams [14–19], where FFLO-type phases were entirely neglected, are qualitatively accurate at least within the mean-field approximation.

Since population imbalance breaks the time-reversal symmetry when $P \neq 0$, the \uparrow and \downarrow fermions again rotates (mostly) in opposite directions with unequal speeds. Similar to the $P = 0$ case, we again see that $|J_\uparrow(r)| \geq J_\downarrow(r)$ has a nonmonotonic dependence on r , and the peak value of $J_\sigma(r)$ increases with increasing α . In Fig. 2, we see that $|L_\uparrow|/N_\uparrow > L_\downarrow/N_\downarrow$ increases from 0 nonmonotonically, and we again expect $|L_\sigma|/N_\sigma$ to be bounded by 0.5 when $\alpha \gg k_F/M$. Having analyzed the $\Delta(r)$, $n_\sigma(r)$ and $J_\sigma(r)$ profiles, and L_σ , next we analyze the quasiparticle/quasihole excitation spectrum of the system.

C. Inner and outer interface modes

In Fig. 4, we show ε_{mn} as a function of m for population-balanced and -imbalanced Fermi gases. First of all, we note that the spectrum satisfies $\varepsilon_{mn} = -\varepsilon_{-m-1,n}$, which follows from the particle-hole symmetry of the parent Hamiltonian. When $P = 0$ and $\alpha = 0$, it is well-known that the quasiparticle and quasihole spectrum are separated with an energy gap around $m \approx 0$. When $P =$ and $\alpha \neq 0$, it is expected that the spectrum splits into two in m space, creating two identical energy gaps located at finite m values. Their locations are approximately symmetric around $m = 0$, and this is clearly seen in Fig. 4(a). For low $P \neq 0$ the spectrum is similar.

When $P \neq 0$ is sufficiently high and α is small, we show in Fig. 4(b) that the continuum of quasiparticle and quasihole spectrum are connected by two discrete branches, i.e. inner and outer interface modes [23]. This indicates that there must be two phase boundaries (interfaces) between a topologically nontrivial superfluid phase and a trivial one. In our case, while the inner mode occurs at the interface between the locally unpolarized or low-polarized superfluid phase existing near the center of the trap and locally high-polarized superfluid phase existing at some intermediate region, the outer mode occurs at the interface between the locally high-polarized superfluid phase and locally spin-polarized normal phase existing near the edge of the system. However, the energy separation between the inner interface modes becomes larger with increasing α , which causes this branch to move completely into the continuum beyond a critical α value. Therefore, for large α , the continuum of quasiparticle and quasihole spectrum are connected by a single branch of outer interface modes. This is clearly seen in Fig. 4(c), and it is a direct consequence of the disappearance of the inner phase boundary, which approximately happens when $\alpha \gtrsim 0.5k_F/M$, as discussed in Sec. III B.

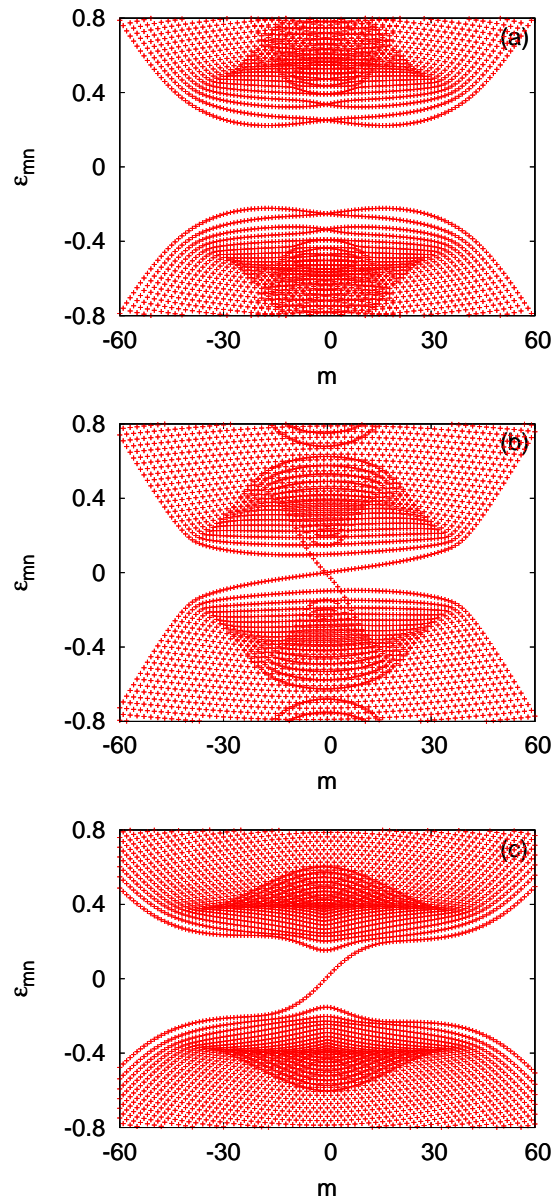


FIG. 4: (color online) We set the two-body binding energy to $|\varepsilon_b| = 0.2\varepsilon_F$, and show the single-particle excitation spectrum ε_{mn} (in units of ε_F) as a function of angular quantum number m . Here, the population-imbalance parameter P and spin-orbit coupling strength α are $P = 0$ and $\alpha = 0.4k_F/M$ in (a), $P = 0.5$ and $\alpha = 0.4k_F/M$ in (b), and $P = 0.5$ and $\alpha = 1.0k_F/M$ in (c).

IV. CONCLUSIONS

To conclude, here we studied harmonically trapped Fermi gases with Rashba-type spin-orbit coupling in two dimensions. We considered both population-balanced and -imbalanced Fermi gases throughout the BCS-BEC evolution, and paid special attention on the effects of spin-orbit coupling on the spontaneously induced countercirculating mass currents and the associated intrinsic angular momentum.

One of our main findings is that even a small spin-orbit cou-

pling destabilizes FFLO-type spatially modulated superfluid phases against the polarized superfluid phase. This suggests that FFLO-type modulated phases, which are known to play a minor role in the thermodynamic phase diagrams when $\alpha = 0$, becomes irrelevant for sufficiently large α . Therefore, we provided supporting evidence that the recent thermodynamic phase diagrams [14–19], where FFLO-type phases were entirely neglected, are qualitatively accurate at least within the mean-field approximation. We also found that the phase separated state rapidly becomes unstable against polarized superfluid phase as α increases from 0, which is in good agreement with recent works on thermodynamic phase diagrams. In addition, we showed for population-imbalanced Fermi gases that the continuum of quasiparticle and quasihole excitation spectrum can be connected by zero, one or two discrete branches of interface modes depending on the particular value of P

and α . The number of branches is determined by the number of interfaces between a topologically trivial phase (e.g. locally unpolarized/low-polarized superfluid or spin-polarized normal) and a topologically nontrivial one (e.g. locally high-polarized superfluid), that may be present in a trapped system.

V. ACKNOWLEDGMENTS

This work is supported by the Marie Curie International Reintegration (Grant No. FP7-PEOPLE-IRG-2010-268239), Scientific and Technological Research Council of Turkey (Career Grant No. TÜBİTAK-3501-110T839), and the Turkish Academy of Sciences (TÜBA-GEBİP).

-
- [1] M. Z. Hasan and C. L. Kane, *Rev. Mod. Phys.* **82**, 3045 (2010).
 - [2] X.-L. Qi and S.-C. Zhang, *Rev. Mod. Phys.* **83**, 1057 (2011).
 - [3] Y.-J. Lin, Y.-J. Lin, K. Jiménez-García, and I. B. Spielman, *Nature (London)* **471**, 83 (2011).
 - [4] S. Chen, J.-Y. Zhang, S.-C. Ji, Z. Chen, L. Zhang, Z.-D. Du, Y. Deng, H. Zhai, and J.-W. Pan, arXiv:1201.6018 (2012).
 - [5] P. Wang, Z.-Q. Yu, Z. Fu, J. Miao, L. Huang, S. Chai, H. Zhai, and J. Zhang, arXiv:1204.1887 (2012).
 - [6] L. W. Cheuk, A. T. Sommer, Z. Hadzibabic, T. Yefsah, W. S. Bakr, and M. W. Zwierlein, arXiv:1205.3483 (2012).
 - [7] E. Cappelluti, C. Grimaldi, and F. Marsiglio, *Phys. Rev. Lett.* **98**, 167002 (2007).
 - [8] J. P. Vyasnakere, S. Zhang, and V. B. Shenoy, *Phys. Rev. B* **84**, 014512 (2011).
 - [9] Z. Q. Yu and H. Zhai, *Phys. Rev. Lett.* **107**, 195305 (2011); H. Zhai, *Int. J. Mod. Phys. B* **26**, 1230001 (2012).
 - [10] Hui Hu, L. Jiang, X.-J. Liu, and Han Pu, *Phys. Rev. Lett.* **107**, 195304 (2011); *Phys. Rev. A* **84**, 063618 (2011).
 - [11] B. Huang and S. Wan, arXiv:1109.3970 (2011); X. Yang and S. Wan, *Phys. Rev. A* **85**, 023633 (2012).
 - [12] S. Takei, C.-H. Lin, B. M. Anderson, and V. Galitski, *Phys. Rev. A* **85**, 023626 (2012).
 - [13] M. Gong, S. Tewari, and C. Zhang, *Phys. Rev. Lett.* **107**, 195303(2011); G. Chen, M. Gong, and C. Zhang, *Phys. Rev. A* **85**, 013601 (2012).
 - [14] M. Iskin and A. L. Subaşı, *Phys. Rev. Lett.* **107**, 050402 (2011); *Phys. Rev. A* **84**, 043621 (2011).
 - [15] W. Yi and G.-C. Guo, *Phys. Rev. A* **84**, 031608(R) (2011).
 - [16] Li Han and C. A. R. Sá de Melo, *Phys. Rev. A* **85**, 011606(R) (2012); Kangjun Seo, Li Han, and C. A. R. Sá de Melo, *Phys. Rev. A* **85**, 033601 (2012).
 - [17] K. Zhou and Z. Zhang, *Phys. Rev. Lett.* **108**, 025301 (2012).
 - [18] R. Liao, Y. Y. Xiang, and W.-M. Liu, *Phys. Rev. Lett.* **108**, 080406 (2012).
 - [19] J. N. Zhang, Y. H. Chan, and L. M. Duan, arXiv: 1110.2241 (2011).
 - [20] J. Zhou, W. Zhang, and W. Yi, *Phys. Rev. A* **84**, 063603 (2011).
 - [21] S. K. Ghosh, J. P. Vyasnakere, and V. B. Shenoy, *Phys. Rev. A*, **84**, 053629 (2011).
 - [22] L. He and X. G. Huang, *Phys. Rev. Lett.* **108**, 145302 (2012); and arXiv:1202.1492 (2012).
 - [23] X.-J. Liu, L. Jiang, Han Pu, and Hui Hu, *Phys. Rev. A* **85**, 021603(R)(2012).
 - [24] M. Feld, B. Frohlich, E. Vogt, M. Koschorreck, and M. Köhl, *Nature* **480**, 75 (2011); E. Vogt, M. Feld, B. Frohlich, D. Pertot, M. Koschorreck, and M. Köhl; *Phys. Rev. Lett.* **108**, 070404 (2012).
 - [25] A. T. Sommer, L. W. Cheuk, M. J.-H. Ku, W. S. Bakr, and Martin W. Zwierlein, *Phys. Rev. Lett.* **108**, 045302 (2012).
 - [26] E. Doko, A. L. Subaşı, and M. Iskin, *Phys. Rev. A* **85**, 053634 (2012).
 - [27] F. Chevy, K. W. Madison, and J. Dalibard, *Phys. Rev. Lett.* **85**, 2223 (2000).
 - [28] P. C. Haljan, B. P. Anderson, I. Coddington, and E. A. Cornell, *Phys. Rev. Lett.* **86**, 2922 (2001).
 - [29] S. Riedl, E. R. Sanchez Guajardo, C. Kohstall, J. Hecker Denschlag, and R. Grimm, *Phys. Rev. A* **79**, 053628 (2009).
 - [30] T. Mizushima, M. Ichioka, and K. Machida, *Phys. Rev. Lett.* **101**, 150409 (2008).